Lung Cancer Segmentation and Classification Using Integration of Convolutional Neural Network & Unet Network Over CT Images: A Deep Learning Approach

Arun B. Mathews [1] & Krishna Prasad K. [2]

[1] Post-Doctoral Research Scholar, Srinivas University, Mangalore, India.
Orcid-ID: 0000-0002-2173-5415, E-mail: marthomat@gmail.com

[2] Associate Professor College of Computer Science and Information Science, Srinivas University, Mangalore, India.
Orcid-ID: 0000-0001-5282-9038; E-mail: krishnaprasadkcci@srinivasuniversity.edu.in

Area/Section: Computer Science.
Type of the Paper: Methodological research.
Type of Review: Peer Reviewed as per |C|O|P|E| guidance.
Indexed in: OpenAIRE.
DOI: https://doi.org/10.5281/zenodo.6781593
Google Scholar Citation: IJMTS

How to Cite this Paper:

Mathews, Arun B., & Krishna Prasad, K., (2022). Lung Cancer Segmentation and Classification Using Integration of Convolutional Neural Network & Unet Network Over CT Images: A Deep Learning Approach. *International Journal of Management, Technology, and Social Sciences (IJMTS)*, *7*(1), 520-534. DOI: https://doi.org/10.5281/zenodo.6781593

International Journal of Management, Technology, and Social Sciences (IJMTS)
A Refereed International Journal of Srinivas University, India.

CrossRef DOI: https://doi.org/10.47992/IJMTS.2581.6012.0206

Received on: 17/04/2022
Published on: 30/06/2022

© With Authors.

This work is licensed under a Creative Commons Attribution-Non-Commercial 4.0 International License subject to proper citation to the publication source of the work.
Disclaimer: The scholarly papers as reviewed and published by the Srinivas Publications (S.P.), India are the views and opinions of their respective authors and are not the views or opinions of the SP. The SP disclaims of any harm or loss caused due to the published content to any party.

Lung Cancer Segmentation and Classification Using Integration of Convolutional Neural Network & Unet Network Over CT Images: A Deep Learning Approach

Arun B. Mathews [1] & Krishna Prasad K. [2]

[1] Post-Doctoral Research Scholar, Srinivas University, Mangalore, India.
Orcid-ID: 0000-0002-2173-5415, E-mail: marthomat@gmail.com

[2] Associate Professor College of Computer Science and Information Science, Srinivas University, Mangalore, India.
Orcid-ID: 0000-0001-5282-9038; E-mail: krishnaprasadkcci@srinivasuniversity.edu.in

ABSTRACT

Purpose: *Cellular breakdown in the lungs screening is a cycle that is utilized to recognize the presence of cancer in the lungs in any case. Mostly it occurs among the elderly, especially smokers. Lung infections are lung-affecting illnesses that impede the respiratory mechanism. Cellulose breakdown in the lungs is one of the top causes of mortality in people all over the globe. Early recognition can improve endurance chances. As the world is revolutionizing with so many emerging technologies and one of the most popular technology is Deep Learning (DL) which has shown tremendous development in medical fields. So this paper brings an effective deep learning framework for lung cancer detection.*

Objective: *To develop a CAD system for efficient lung cancer detection from CT images using a combination of CNN and UNET. For improving accuracy in the proposed system a better feature extraction and feature selection techniques is incorporate, i.e., by using autoencoder and selection based on Kernal function for effective boostings.*

Methodology: *For this deep learning framework, the following are the stages. (a) Data Collection from the popular repository IQ-OTHNCCD lung cancer dataset which contains CT images of a total of 1198 from 110 CT slice cases, (b) Preprocessing CT images with an alpha-trimmed mean filter and CLAHE for improved enhancement, (c) Segmentation using CNN for segmenting the cancer regions) with the use of an autoencoder, extracting characteristics like area, perimeter, centroid, and mean intensity) feature selection using kernel function and finally f) classification using UNet network.*

Findings/Result: *In terms of accuracy, sensitivity, specificity, recall, precision, F1-score, detection rate, TPR, FPR, and computation time, experiments are carried out on a range of cutting-edge models, and our suggested model surpasses them all (accuracy:0.95, sensitivity:0.97, specificity:0.98, detection rate:0.94).*

Originality: *This paper is incorporating 2 neural networks over main stages such as segmentation and classification which eventually improves the quality of the model higher and also these are performed over real-time public medical records which shows the novelty of the model.*

Paper type: *Methodology paper*

Keywords: Convolutional Neural Network, CT images, Classification, Deep learning, Lung Cancer, Segmentation, UNet

1. INTRODUCTION :

Lung cancer is the most common cancer in both men and women, and it is also the leading cause of death globally [1-5]. In 2015, lung cancer would account for 13% of all cancer cases, with 200 new cases, according to some estimates. Lung cancer (Figure 1) is responsible for about a quarter of all cancer fatalities. As a result, early detection of lung nodules necessitates evaluation and ongoing monitoring. Individuals with lung cancer can improve their 5-year survival rate by around 50% if they are discovered early [6, 7]. Computable tomography is an efficient technology for identifying lung

nodules because it can provide three-dimensional images of the chest. As a result, the pathophysiology of nodules and tumours is better understood. A CT scan combined with computer processing is frequently utilised in clinics to enhance lung nodule diagnosis. The computer-aided diagnosis of lung cancer comprises a detection system known as CADe and a diagnostic system known as CADx. In the previous phase, CADe was utilised to categorise potential nodules as nodules or non-nodules. This technology is used to identify benign and malignant nodules [8-10]. The size, shape, and appearance of lung nodules are associated with the risk of malignancy, CADx can identify benign and malignant pulmonary nodules based on texture, shape, and development rate. As a result, the accuracy, speed, and automation of a CADx system can all be quantified.

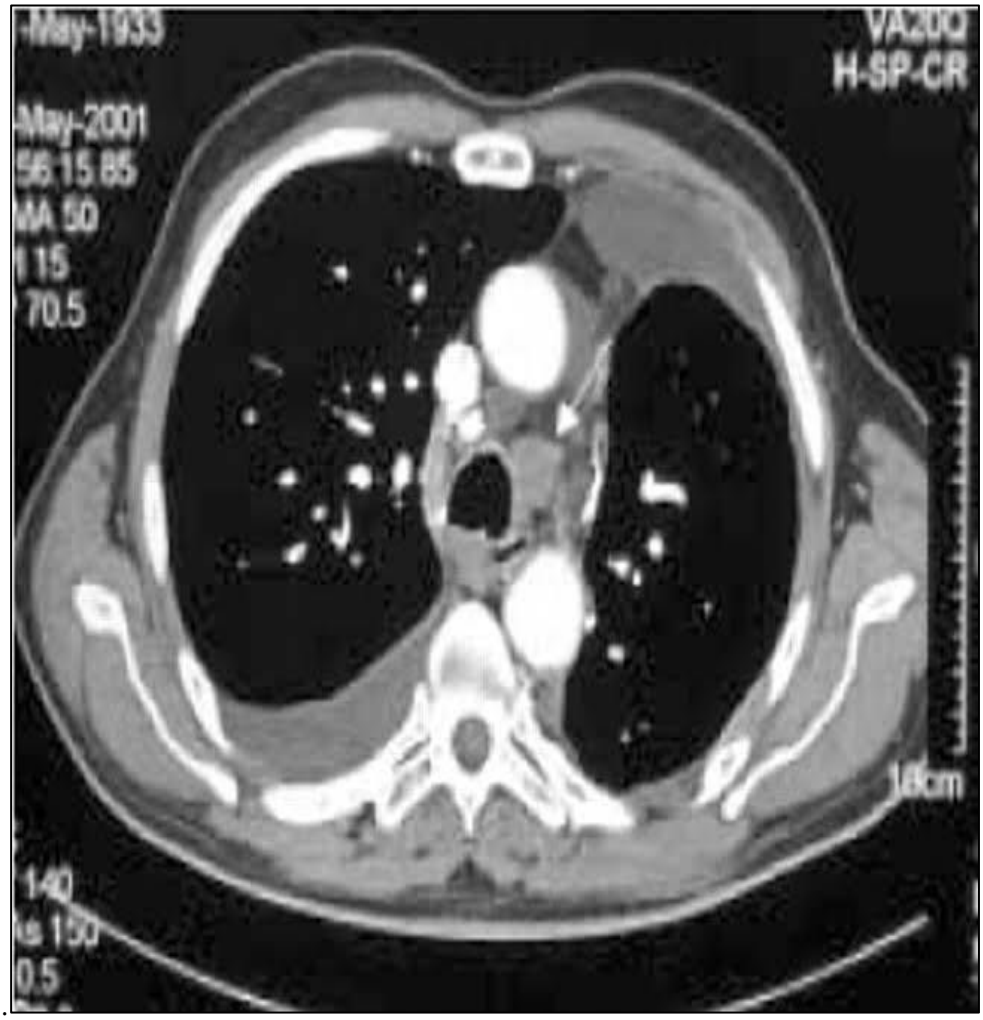

Fig. 1: Staging of lung cancer: CT image [32]

Several researchers have recently advocated utilising Artificial Intelligence (AI), namely Deep Learning, to define pulmonary nodules, possibly lowering the number of scans necessary to determine if a tumour is benign or malignant. The majority of these investigations included nodules with sizes of up to 30 mm, indicating that these methods' sensitivity is restricted [11, 12]. Since most lung malignancies are bigger than benign nodules, data sets with large nodules are skewed. Therefore deep learning frameworks have shown such revolutionized development in the medical field.

2. LITERATURE REVIEW :

Coudray et al. (2018) used images from The Cancer Genome Atlas to construct a deep convolutional neural network which automatically classified them as LUAD, LUSC or normal lung tissue and gave accurate results. Our technique performs with an average area under the AUC curve of 0.97. To identify lung cancer from CT data, Bhatia et al. (2019) also used deep residual learning methods [13]. They use

the UNet and ResNet models to highlight cancer-prone lung regions and extract features, and they present many preprocessing ways for doing so [11].

Abdullah et al. (2021) [1], who examined multiple machine learning algorithms for lung cancer detection, employed the feature set. There have been an overwhelming number of methods for diagnosing lung cancer in recent years, the bulk of these use CT scan images, although others use x-ray scans. Furthermore, a range of classifier systems is coupled with a variety of segmentation approaches to apply image recognition to locate lung cancer nodules. Chen et al. (2021) employed a unified memory method to get over compute accelerator memory restrictions. Tian et al. looked at PD-L1 expression in 939 patients with stage IIIB-IV NSCLC who had CT scans before treatment (2021). CT images from the test cohort (n= 96) were utilised to train and optimise a deep Convolutional Neural Network, whereas CT images from the training (n= 750) and validation (n= 94) cohorts were used to discover the PD-L1 expression signature (PD-L1ES). Finally, the predictive utility of PD-L1ES in terms of clinical outcome was investigated using a different immunotherapy cohort (n=94) [10].

3. OBJECTIVES :

To develop an efficient lung cancer detection technique by using the CT images with a combination of CNN and UNET. To improve the accuracy by using a better feature extraction and feature selection techniques is incorporate, i.e., by using autoencoder and selection based on Kernal function for effective boostings.

Organization of paper: The following is a breakdown of the rest of the article: Sections 2 and 3 provide the literature review, methodology, and performance analysis. Section 5 concludes the paper.

4. METHODOLOGY :

Figure 2 depicts the overall architecture of the proposed system in which the following are the stages. (a) Data Collection from the repository OTHNCCD lung cancer dataset which contains CT images of a total of 1198 from 110 CT slice cases. Once these images are collected, they are passed over, (b) Preprocessing stage was from raw images, and the possibility of noises and anomalies is higher. CLAHE was used to remove the Alpha-trimmed mean filter and improve the image quality. Once these images are been preprocessed, they will be given for, (c) segmentation where cancer regions of interest are segmented using CNN and then, (d) feature extraction for extracting quintessential features (area, perimeter, centroid, diameter, eccentricity and mean intensity) with the help of auto-encoder and from those, (e) feature selection for selecting quintessential features using Kernel function and finally given for, (f) classification were UNet gives hands for classifying the CT images.

4.1 Data Collection:

In the autumn of 2019, the lung cancer dataset for the Iraq-Oncology Teaching Hospital/National Center for Cancer Diseases (IQ-OTH/NCCD) was gathered across three months in the aforementioned specialised institutions. CT scans of lung cancer patients at various stages, as well as healthy persons, were included in the research. Oncologists and radiologists from these two institutions labelled the IQ-OTH/NCCD slides. There were 1190 images in the collection, which exhibit CT scan slices from 110 separate instances (see Figure 3). Normal, benign, and malignant examples are the three categories of situations. There were 40 malignant cases, 15 benign cases, and 55 non-cancerous ones. Initially, the CT scans were saved in DICOM format. In this experiment, a Siemens SOMATOM scanner was employed. The following CT protocol was utilised for reading: 120 kV, 1 mm slice thickness, window widths between 350 and 1200 HU, and window centres between 50 and 600. Before processing, all images were de-identified. The oversight review board did not require written consent. The institutional review boards of the participating medical centres gave their approval to the study. There were multiple slices in each scan. The number of slices ranged between 80 and 200, and each one showed a different side and viewpoint of the human chest. Gender, age, educational achievement, home location, and living situation were all different in each of the 110 instances. Few work for Iraq's transportation and oil ministries, while others worked as farmers and gainers. They mostly hailed from Iraq's central region, including Baghdad and Babylon provinces.

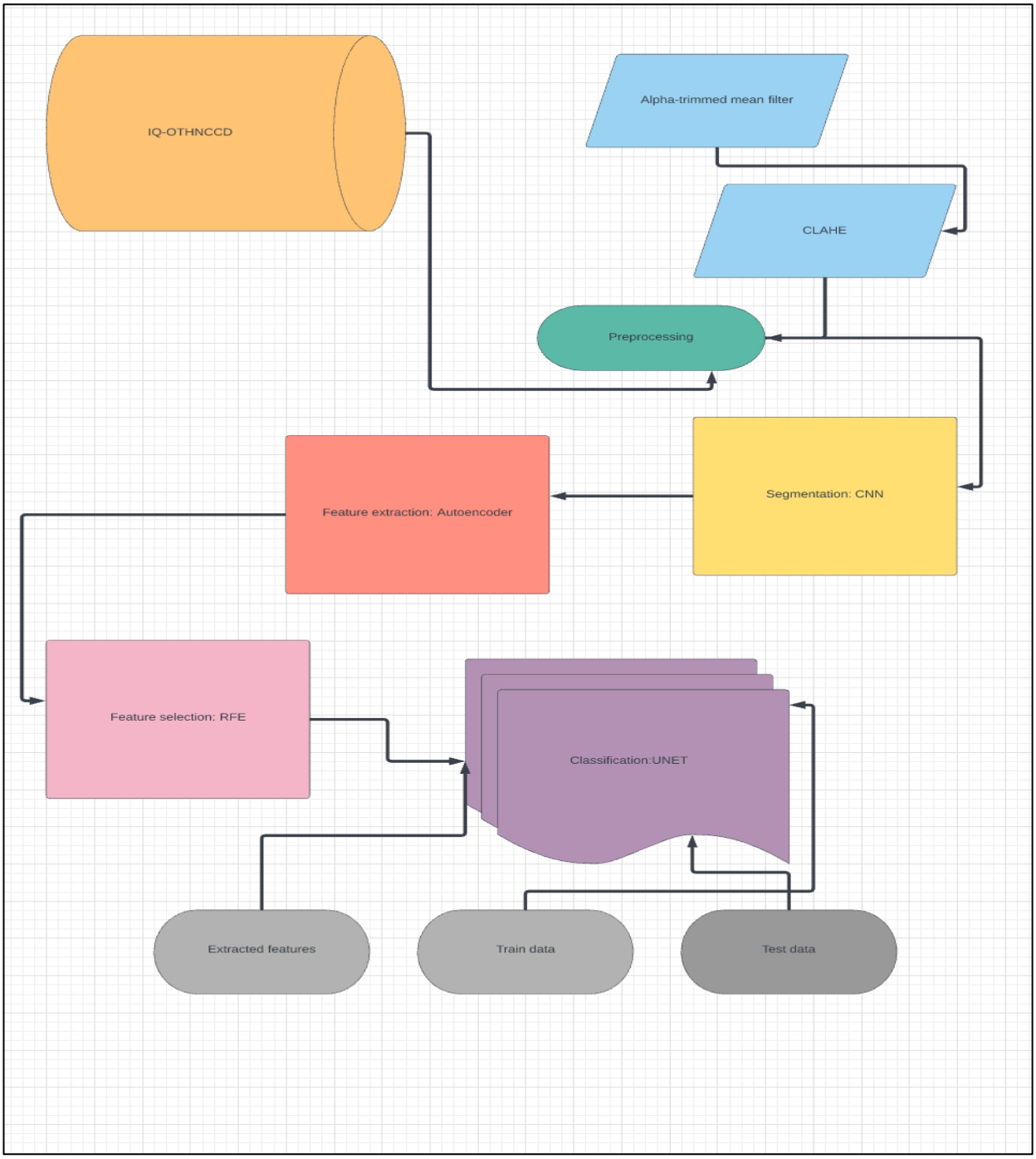

Fig. 2: The overall architecture of the proposed framework

4.2 Preprocessing:

Preprocessing stage is one of the most important stages used for the removal of noises and anomalies from the raw inputs and to enhance the image for further process. We employed the Alpha-trimmed mean filter and CLAHE approaches for this.

4.2.1 Alpha-trimmed Mean Filter

The mean filter with alpha trimming, which combines mean and median filters, is a hybrid of the two. On a structural element, place a mask (3x3, 5x5). Then arrange the pixel components in a logical arrangement. The first and last pixels in the order list should be discarded. Calculate the average for the order list that hasn't been filled yet. The number of elements of records to be discarded is represented by the alpha here. When the alpha parameter is set to 0, the mean filter that has been Alpha-trimmed

degenerates into a mean filter. Filter windows size minus 1 is the maximum value of alpha, and the mean filter degenerates into a median filter [7].
Assuming {x(i), x(i – 1), ... x(i – n + 1)} as a collection of n samples signal values seen in windows W, where n=2N+1.The output of this shown below:

$$y(i,\alpha) = \frac{x}{n-2[\alpha n]} \sum_{j=\{\alpha n\}+1} x_j(i) \quad \text{--------} \quad (1)$$

where [x] is the largest integer component and 0 < 0.5

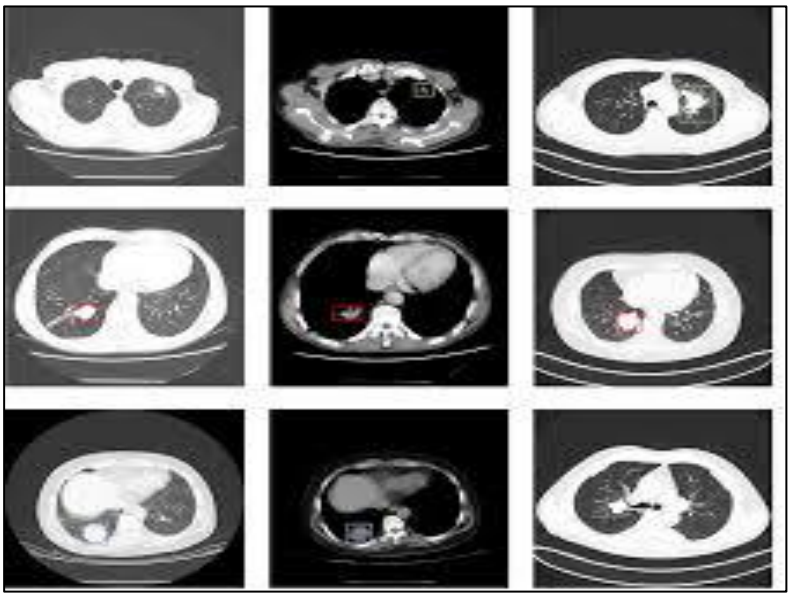

Fig. 3: Instances of IQ-OTHNCCD dataset CT images [11-14]

4.2.2 Image Enhancement

CLAHE and Adaptive Histogram Equalization employ a variety of approaches to deal with noise amplification [31]. CLAHE separates the input image into non-overlapping contextual portions (also known as sub-images, tiles, or blocks), performs histogram equalisation on each, clips the original histogram to a certain value, and the clipped pixels are then redistributed to each grey level. The contextual region's Block Size (BS) is generally selected at the point where the entropy curvature is maximal 33. Although the BS is computed empirically in 16x16 pixels, the Clip Limit (CL) for the computations is 0.01 (as defined in Ref. [13]). The intensity of each pixel in the redistributed histogram is limited to a maximum value, unlike the normal histogram. The lowest and highest grey levels in the original and altered images, on the other hand, are identical. We chose a uniform distribution to optimise the intensity levels in each contextual zone since it has been observed to produce better outcomes, as stated in Ref. [21]. Finally, boundary artefacts are removed by determining the new grey level assignment of the pixels through a bilinear interpolation between four possible mappings inside a sub-matrix contextual area.CLAHE has been utilised in medical imaging to increase contrast. CLAHE-DWT, which combines CLAHE with DWT to reduce contrast overstretching and noise enhancement concerns, was presented by Huang to solve CLAHE's shortcomings. This is crucial since the image's brightness does not require as much adjustment as the image's blackness. CLAHE is used in conjunction with FABEMD and HMF in the proposed approach to stabilise and preprocess the image before applying CLAHE, making use of the former's direct component segmentation capabilities and the latter's corrective advantages. Figure 4 shows the results of CLAHE-based CT scans [25, 20] [17, 18].

4.3 Segmentation:

A simple CNN model that can identify actual lung cancer and lung image patches were proposed. With a convolutional layer, an image input layer, a pooling layer, and a Softmax layer, this CNN network contains two totally linked layers. The CNN model is shown in its entirety in Figure 5. We only have one convolutional layer with six convolutional kernels to cope with the input set of 32 image patches, as opposed to the well-known AlexNet structure, which has five. SGD convergence is improved and overfitting is avoided using the Rectified Linear Unit (ReLU) and normalisation layers that follow the

single convolution layer. MaxPooling is the first completely linked layer, followed by a dropout layer, ReLU, and Softmax. A total of 120 neurons make up the first Fully Connected layer (FC). Overfitting may be avoided with the aid of the dropout layer [19].

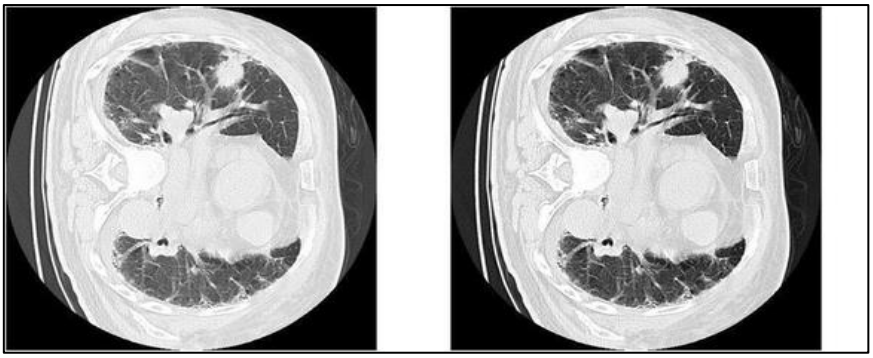

Fig. 4: Original CT image (left) and its CLAHE based CT (right) [17]

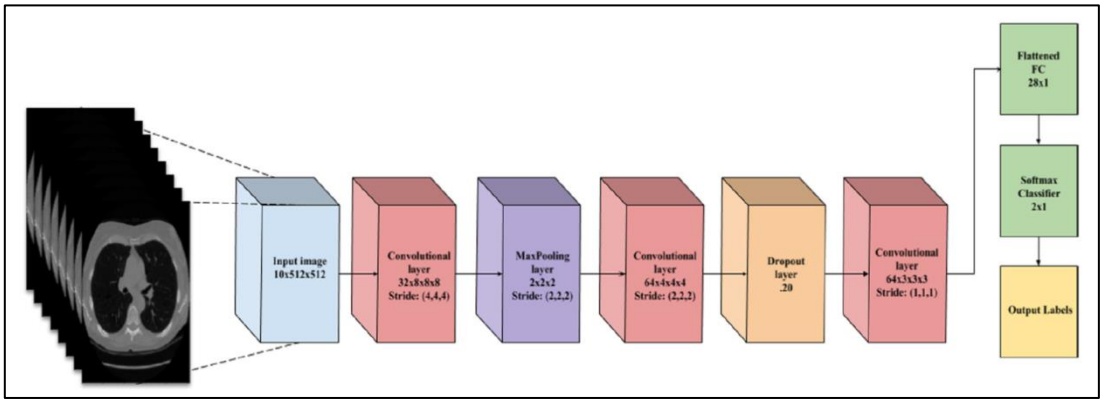

Fig. 5: Segmentation using CNN [19]

The CT images are sent into the trained CNN after being segmented into 32× 32 patches with each voxel as the centre point. Simultaneously, a label of 1 or 0 will be applied to each patch, indicating whether it is for lung cancer (LC) or non-lung cancer (NLC) [26-29]. To retrieve the whole LP volume, the maximum linked component detection is used. To achieve the final lung cancer segmentation findings, the hole in the LC volume is filled.

4.4 Feature Extraction:

4.4.1 Decomposition

It is useful and practicable to decompose a lung image into tiny patches for identifying key issues and deleting extraneous ones. Pi is an image patch collection, where n is the number of local patches, that may be utilised to create the lung nodule image x shown in Eqn (1):

$$X = [P1, P2, \ldots\ldots\ldots\ldots Pn]$$

Generation determines the placement and size of local patches. The worthless component will be contained in a large patch, a small patch, on the other hand, may not be large enough to cover all of the important issues. Superpixel is a common way of dividing an image into tiny, comparable sections that are more representative and have higher integrity. As a result, it is used in this project.

When deciding if an image patch is suitable for local feature extraction, there are a few more factors to consider:

- Allow Pi to be a local patch, the patch will be removed if its area exceeds Amin or falls below Amax.
- Assume Pi and Pj as 2 local patches. If their intersection and union ratios are larger than Ot, the smaller of the two gets eliminated. Amin, Amax, and Ot are predefined thresholds [23, 24, 30].

4.4.2 Autoencoder

Using unlabeled data to extract features using an autoencoder has become a realistic alternative due to the recent rapid increase in unsupervised learning. A multilayer neural network is used in the autoencoder model. It was designed as a forward network with a single hidden layer at the beginning. Allow xi to represent input data, a_{ij} to represent unit activation in layers I and j, and wi to represent the weights matrix controlling the function mapping from layer I to layer i+1. If layer I contain si units and layer i+1 includes si+1 units, Wi is a matrix with si*si+1 dimensions. In Eqn (2), where a_{i2} is the initial unit of the second layer and x3–x0 are the four input features: [24, 25]

$$a_1^2 = g(w_{10}^1 x_0 + w_{11}^1 x_1 + w_{12}^1 x_2 + w_{13}^1 x_3) \quad \text{-----} \quad (2)$$

The output of an autoencoder is always the same as or equal to the input. Everything is based on a formula that goes like this:

$$a = h(x) = f\left(W^E x + b\right)$$
$$x' = h'(x) = g\left(W^D a + b'\right)$$
$$= g\left(W^D h(x) + b'\right) \quad \text{------} \quad (3)$$

The encoder and WD decoder weight matrices are respectively X' and We. To activate the units in each layer, use the sigmoid or tan h activation functions f(.) and g(.). As x approaches, x', an abstract and compressed output feature vector x should be able to rebuild the input feature. The following is a general definition of the cost function:

$$J(W, b) = \frac{1}{N}\sum_{i=1}^{\frac{1}{2}} \|x_i' - x_i\|^2 + \lambda \sum_{l=1}^{N_l - 1} \sum_{i=1}^{M_i} \sum_{j=1}^{M_{i+1}} \left(W_{ij}^l\right)^2 \quad \text{----} \quad (4)$$

By stacking additional hidden layers, a deep autoencoder may be created. The model has five layers, as seen in Figure 4 (including 3 hidden layers). The layers L1 to L3 for encoding and L3 to L5 for decoding. Li is used as the input of the layer Li+1, and the weights can be gained based on equation (3). There are 2 stacked autoencoders. The activation of 1st hidden layer is the input of the 2nd stacked autoencoder. The network can be trained in a fine-tuning stage by minimizing the equation (4). W1 and W4 are trained using the 1st stacked autoencoder's encoding and decoding weights, whereas W2 and W3 are trained using the 2nd stacked autoencoder's encoding and decoding weights. Finally, the entire network may be built in a layered manner, layer by layer. Figure 6 depicts one type of symmetric encoding and decoding scheme, although other layouts are also possible.

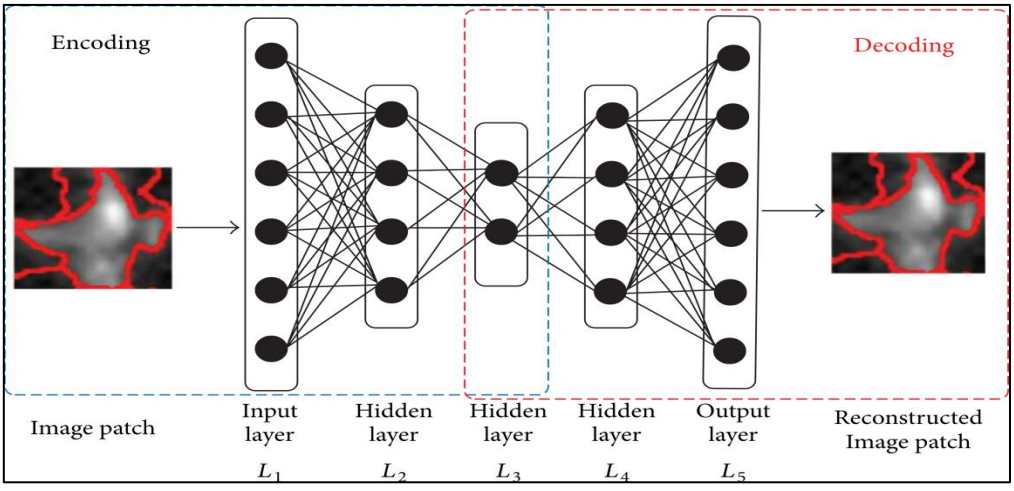

Fig. 6: Autoencoder for feature extraction [23]

A deep autoencoder model may thus be used to represent each local patch of a lung nodule image Pi as a fixed-length feature vector Pfi. Then Eqn (1) is rewritten as follows:

X = [P1, P2, ...Pn]
= [Pf1, ...Pfk]

4.5 Feature Selection:

The kernel function was created by Vapnik [28], and it was later modified by Schokopf et al., Christiani and Taylor, and others. The dot product xkt, x_i is mapped to Φ(xkt) Φ(xi). Mercer's Theorem defines the kernel function as follows [14] [18, 26]:

$$K(x_i^T x_i) = \phi(x_i)^T \phi(x_i) \quad (5)$$

There are various sorts of kernel functions. Gaussian, polynomial, and other types of models exist. The following formula may be used to compute Euclidean distance:

$$\begin{aligned} \|\phi(x_b) - \phi(x_i)\|^2 &= (\phi(x_z) - \phi(x_i))^{\dagger}(\phi(x_b) - \phi(x_i)) \\ &= K(x_b x_b) - 2K(x_b x_i) + K(x_i, x_i) \end{aligned} \quad (6)$$

Equation (7) was used to investigate feature selection function dissimilarity using a Gaussian Kernel:

$$K(x_i^T x_i) = \exp\left(-\frac{|W_i^T - x_i^2|^2}{x_A^2}\right) \quad (7)$$

The main concept behind using a kernel function to choose features is to give each feature a weight in order to maximise the goal function g. The formula ek= 1/p', where k=1,2,....p first, will be used to compute Dataset X € Rnxp.The entire no of samples is represented by n, while the total number of genes is represented by p.In order to be classified, the dataset must be labelled, yi € Y, where Y=1,2,.....N. Because the C class will be regarded as a cluster, equation (4) may be used to get the cluster centre Vi=[vi1,.....vip]:

$$v_{ik} = \frac{\Sigma_r \mu_i I_k}{K_i}, \text{where i is assigned as } 1,2,-,C, \text{and j assigned as } 1,2,-,n \quad \text{-----} \quad (8)$$

The Ci class's total number of samples is denoted by the letter C. The kernel function will be used to calculate the feature selection dissimilarity measure. The following is the function of dissimilarity estimated using kernel (9) between the sample and the cluster's centre:

$$\| \phi(x_k) - \phi(x_i)|^2 = 2(1 - X(x_k, v_i)) = 2\left(1 - ex_p\left(-\frac{|x_i - x_i|}{2d^2}\right)\right) \quad \text{-----} \quad (9)$$

In SCAD as a feature selection process, the target function is equivalent to the goal function, as shown in equation [10]:

$$\begin{aligned} &\min\ J = \sum_{i=1}^{c} \sum_{xj \in C_i} \phi^2(x_j, v_i) + \delta \sum_{k=1}^{p} w_k^2 \\ = &\sum_{i=1}^{c} \sum_{xj \in c_i} \sum_{k=1}^{p} w_k \| \phi(x_{jk}) - \phi(v_{jk})||^2 + \delta \sum_{k=1}^{p} w_k^2 \end{aligned}$$

Here $w = (w_1, w_1, \dots, w_p)$ subject to

$$\begin{cases} w_k \in [0,1], k = 1, \dots., p \\ \sum_{k=1}^{p} w_k = 1 \end{cases} \quad \text{------} \quad (10)$$

Make the value of wk and delta the smallest to minimise the objective function. To attain the lowest of δ and wk, the values of δ and wk must be altered. Equation (11) and equation (12) illustrate the objective function for updating:

$$w_k = \frac{1}{p} + \frac{1}{2\delta} \sum_{i=1}^{C} \sum_{x_j \in c_i} \left| \frac{\sum_{k=1}^{i} |\Phi(x_{jk}| - \Phi(v_{ik}\|}{p} - \|\phi(x_{jk}) - \phi(v_{ik})\|^2 \right| \quad \text{------} \quad (11)$$

$$\delta^t = \frac{a \sum_{i=1}^{C} \sum_{x_j c_i} \sum_{k=1}^{p} w_k^{t-1} \|\phi(x_{jk}) - \phi(v_{ik})^2}{\sum_{k=1}^{p} (w_k^{t-1})^2}, \text{ a constant} \quad \text{--------} \quad (12)$$

4.6 Classification:

The edge of the observed item (lung cancer) is generally changing in biomedical images, and the intricate patterns of the imaged object (lung cancer) are common. Long et al. developed a new technique for deep decoding by integrating the high-level representation of deep decoding layers with the appearance representation of shallow encoding levels. [6 & 8] suggested using skip-architecture to provide exact categorization for objects with intricate patterns. This method has been shown to work with natural images [20] and might be used for biomedical images as well. The U-Net, a skip-

architecture-based cell tracking technique, was introduced by Ronneberger et al. The U-Net, which has two paths: down-sampling and up-sampling, provides support for our network (decoding). In the downsampling method, 5 convolutional blocks are used. Each block has two convolutional layers, one with 10× 24 feature mappings and the other with a 3×3 filter size, one stretch in both directions, and rectifier activation. Downsampling drops feature maps from 240× 240 to 15× 15 by extending stride 2×2 to the end of each block except the last one. Each upsampling block begins with a deconvolutional layer with a filter size of 3x3 and a stride of 2x2, increasing the size of feature maps in both directions while decreasing the number of feature maps by two, resulting in 240x240 feature maps. To minimize the number of feature maps produced, each up-sampling block contains two convolutional layers that concatenate deconvolutional feature maps with feature maps from the encoding route. In contrast to the original U-Net architecture, we use zero padding for all convolutional layers in down and up-sampling routes. Lastly, a 1× 1 feature mapping layer decreases the no: of feature mappings to two: one for the foreground and the other for the backdrop. The network has nil layers that are fully linked. In Table 1, you'll find more network settings [15] [24] [22].

Table 1: Overall parameters of UNET

Parameters	Values
No of convolutional blocks	**[4,5,6]**
No of deconvolutional blocks	**[4,5,6]**
Regularization	**L1,L2,Dropout**

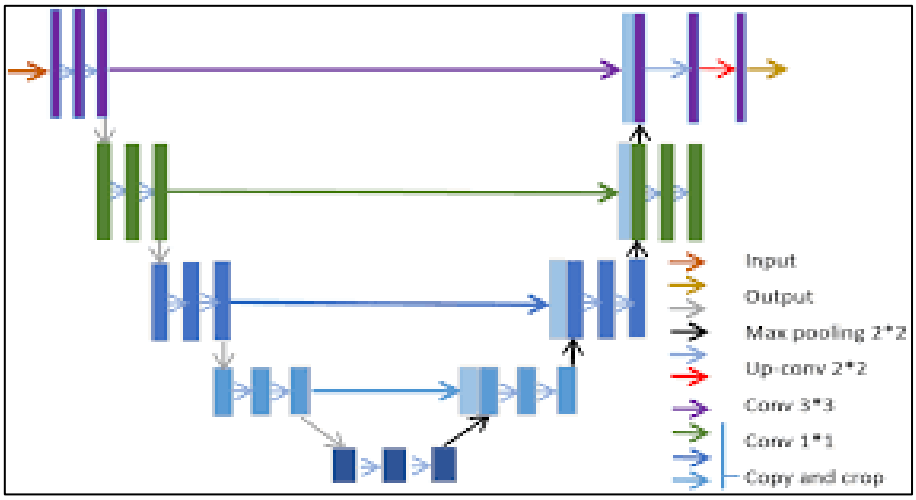

Fig. 7: UNet network for classification of lung cancer [24]

5. PERFORMANCE ANALYSIS :

The implementation of the model is done using hardware specifications like 12th Gen Intel Core i7 and Core i9, Nvidia RTX 3080 Ti, 1 TB HDD, and Windows 10 OS. PyTorch, an open-source python library for generating deep learning models, and Google Collaboratory, an open-source Google environment for developing deep learning models are made use of as software requirements. Experiments are carried out to evaluate the accuracy, sensitivity, specificity, recall, precision, F1-score, detection rate, TPR, FPR, and calculation time of several models, including CNN, VGG16, VGG19, Alexnet, Resnet50, Googlenet, and Inception v3. Table 2 summarizes the study's findings concerning the accuracy, sensitivity, and specificity. Figure 8 depicts a graphical representation of many models, with ours outperforming all of them (accuracy: 0.95, sensitivity:0.97, specificity:0.98).
Table 3 depicts the overall analysis under precision, recall and F1-score. Figure 9 shows the graphical representation of various models over the proposed method in which our model outperforms. Precision, recall and F1-score values are 0.93, 0.87 and 0.90 respectively.

Table 2: Overall analysis under accuracy, sensitivity, specificity

Models	Accuracy	Sensitivity	Specificity
VGG16	84	90	94
VGG19	86	92	96
Alexnet	80	86	89
Resnet50	79	85	90
Googlenet	85	91	94
Inception v3	88	94	96
CNN-UNET	95	97	98

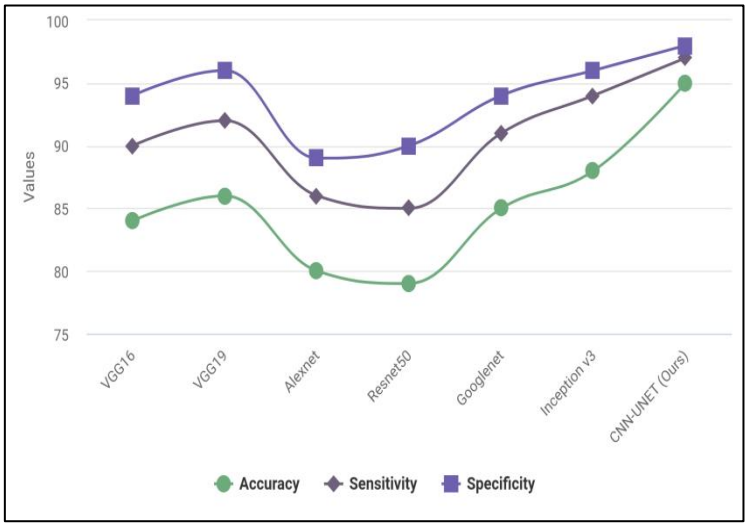

Fig. 8: Models vs Accuracy, Sensitivity and Specificity

Table 3: Overall analysis under precision, recall, and F1-score

Models	Precision	Recall	F1-score
VGG16	84	81	80
VGG19	86	83	84
Alexnet	81	82	80
Resnet50	80	77	81
Googlenet	87	83	84
Inception v3	89	85	88
CNN-UNET	93	87	90

Fig. 9: Models vs Precision, Recall and F1-score

Table 4 depicts the overall analysis under detection rate, TPR and FPR. Figure 10 depicts the overall analysis of various models over the proposed method in which our model outperforms (detection rate:0.94, TPR:0.95, FPR:0.5). Figure 11 illustrates the overall computation time taken during the time of training of models.

Table 4: Overall analysis under detection rate, TPR and FPR

Models	Detection rate	TPR	FPR
VGG16	85	82	18
VGG19	88	86	14
Alexnet	79	73	27
Resnet50	75	70	30
Googlenet	84	80	20
Inception v3	87	86	14
CNN-UNET	94	95	5

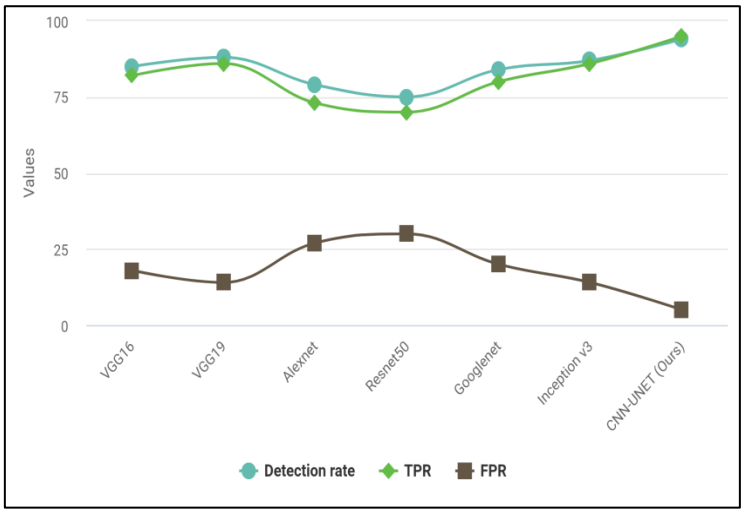

Fig. 10: Models vs Detection rate, TPR, FPR

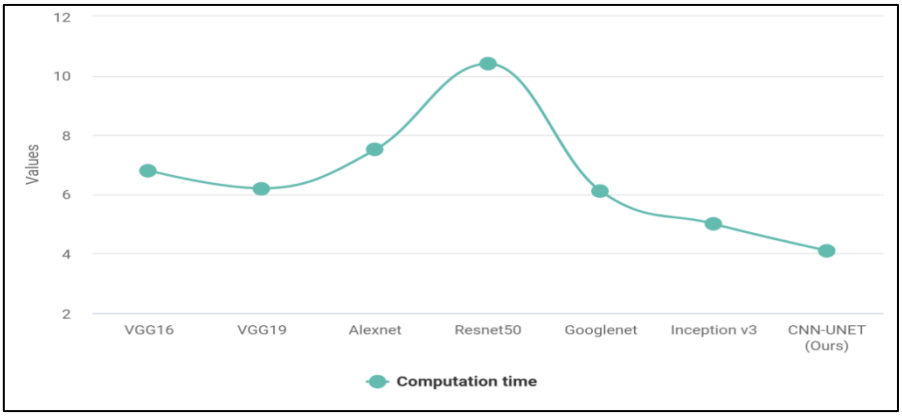

Fig. 11: Models vs Computation time

6. CONCLUSION :

This paper aims in developing an effective deep learning model for lung cancer detection. This paper brings a double deep learning framework where we use a network for both segmentation and classification stages. Initially dataset are collect from popular repository OTHNCD and the no of data considered is 1198 from 100 image slices. This data is preprocessed using CLAHE to remove noise and other anomalies and its followed by segmentation from the segmented image quintessential feature such as area, perimeter, centroid, diameter, eccentricity and mean intensity were extracted and final features selected using Kernel function are fed to the classifier, for effective classification with UNET network. Experimental evaluation states the better performance of proposed model with 95% of accuracy. Future

work will be that, this paper will be helpful for other research specialists to dig deep into understanding and also come up with a more advanced model for effective detection. Also, with more advanced algorithm over classifiers and selection stages helps to bring even more effective results than we expected.

7. RECOMMENDATION :

Future work can be focused on the different deep learning algorithms, with the objective to reduce the computational time and to improve better accuracy. Different experimental parameters can be used to evaluate the effectiveness of the system. A combination of hybrid structures can also be used to improve the efficiency of the system.

REFERENCES :

[1] Abdullah, D. M., & Ahmed, N. S. (2021). A review of most recent lung cancer detection techniques using machine learning. *International Journal of Science and Business*, *5*(3), 159-173. Google Scholar↗

[2] Achanta, R., Shaji, A., Smith, K., Lucchi, A., Fua, P., & Süsstrunk, S. (2012). SLIC superpixels compared to state-of-the-art superpixel methods. *IEEE transactions on pattern analysis and machine intelligence*, *34*(11), 2274-2282. Google Scholar↗

[3] Alakwaa, W., Nassef, M., & Badr, A. (2017). Lung cancer detection and classification with 3D convolutional neural network (3D-CNN). *Lung Cancer*, *8*(8), 409-430.Google Scholar↗

[4] Al-Yasriy, H. F., & Muayed, A. H. (2020). The IQ-OTHNCCD lung cancer dataset. *Mendeley Data*, *1*(1), 1-13. Google Scholar↗

[5] Ardila, D., Kiraly, A. P., Bharadwaj, S., Choi, B., Reicher, J. J., Peng, L., ...& Shetty, S. (2019). End-to-end lung cancer screening with three-dimensional deep learning on low-dose chest computed tomography. *Nature medicine*, *25*(6), 954-961. Google Scholar↗

[6] Astaraki, M., Toma-Dasu, I., Smedby, Ö., & Wang, C. (2019, October). Normal appearance autoencoder for lung cancer detection and segmentation. In *International Conference on Medical Image Computing and Computer-Assisted Intervention*, 249-256. Springer, Cham. Google Scholar↗

[7] Avinash, S., Manjunath, K., & Senthilkumar, S. (2017, May). Analysis and comparison of image enhancement techniques for the prediction of lung cancer. In *2017 2nd IEEE International Conference on Recent Trends in Electronics, Information & Communication Technology (RTEICT)*, 1535-1539. IEEE. Google Scholar↗

[8] Baldwin, D. R., Gustafson, J., Pickup, L., Arteta, C., Novotny, P., Declerck, J., ...& Gleeson, F. V. (2020). External validation of a convolutional neural network artificial intelligence tool to predict malignancy in pulmonary nodules. *Thorax*, *75*(4), 306-312. Google Scholar↗

[9] Bhatia, S., Sinha, Y., & Goel, L. (2019). Lung cancer detection: a deep learning approach. In *Soft Computing for Problem Solving*, 699-705. Springer, Singapore. Google Scholar↗

[10] Chen, C. L., Chen, C. C., Yu, W. H., Chen, S. H., Chang, Y. C., Hsu, T. I., ... & Chen, C. Y. (2021). An annotation-free whole-slide training approach to pathological classification of lung cancer types using deep learning. *Nature communications*, *12*(1), 1-13. Google Scholar↗

[11] Chen, W., Wei, H., Peng, S., Sun, J., Qiao, X., & Liu, B. (2019). HSN: hybrid segmentation network for small cell lung cancer segmentation. *IEEE Access*, *7*(1), 75591-75603. Google Scholar↗

[12] Ciompi, F., Chung, K., Van Riel, S. J., Setio, A. A. A., Gerke, P. K., Jacobs, C., ... & Van Ginneken, B. (2017). Towards automatic pulmonary nodule management in lung cancer screening with deep learning. *Scientific reports*, *7*(1), 1-11. Google Scholar↗

[13] Coudray, N., Ocampo, P. S., Sakellaropoulos, T., Narula, N., Snuderl, M., Fenyö, D., ...& Tsirigos, A. (2018). Classification and mutation prediction from non–small cell lung cancer

histopathology images using deep learning. *Nature medicine*, *24*(10), 1559-1567. Google Scholar↗

[14] Cristianini, N., & Shawe-Taylor, J. (2000). *An introduction to support vector machines and other kernel-based learning methods*. Cambridge university press. *1*(1), 1299–1319. Google Scholar↗

[15] Drozdzal, M., Vorontsov, E., Chartrand, G., Kadoury, S., & Pal, C. (2016). The importance of skip connections in biomedical image segmentation. In *Deep learning and data labeling for medical applications*, 179-187. Springer, Cham. Google Scholar↗

[16] El-Baz, A., Beache, G. M., Gimel'farb, G., Suzuki, K., Okada, K., Elnakib, A., ...& Abdollahi, B. (2013). Computer-aided diagnosis systems for lung cancer: challenges and methodologies. *International journal of biomedical imaging*, 1(1), *1-46*. Google Scholar↗

[17] Farag, A., Elhabian, S., Graham, J., Farag, A., & Falk, R. (2010). Toward precise pulmonary nodule descriptors for nodule type classification. In *Medical image computing and computer-assisted intervention: MICCAI*, *13*(3), 626-633. Google Scholar↗

[18] Hasri, N. M., Wen, N. H., Howe, C. W., Mohamad, M. S., Deris, S., & Kasim, S. (2017). Improved support vector machine using multiple SVM-RFE for cancer classification. *International Journal on Advanced Science, Engineering and Information Technology*, *7*(4-2), 1589-1594. Google Scholar↗

[19] Jena, S. R., & George, S. T. (2020). Morphological feature extraction and KNG-CNN classification of CT images for early lung cancer detection. *International Journal of Imaging Systems and Technology*, *30*(4), 1324-1336. Google Scholar↗

[20] Kareem, H. F., AL-Husieny, M. S., Mohsen, F. Y., Khalil, E. A., & Hassan, Z. S. (2021). Evaluation of SVM Performance in the Detection of Lung Cancer in Marked CT Scan Dataset. *Indonesian Journal of Electrical Engineering and Computer Science*, *21*(3), 1731-1738. Google Scholar↗

[21] Long, J., Shelhamer, E., & Darrell, T. (2015). Fully convolutional networks for semantic segmentation. In *Proceedings of the IEEE conference on computer vision and pattern recognition*, 3431-3440. Google Scholar↗

[22] Peschl, H., Han, D., Van Ooijen, P., Oudkerk, M., Dorrius, M., Rook, M., ...& Gleeson, F. (2018). MA20. 10 Lung Cancer Prediction Using Deep Learning Software: Validation on Independent Multi-Centre Data. *Journal of Thoracic Oncology*, *13*(10), 419-428. Google Scholar↗

[23] Punithavathy, K., Ramya, M. M., & Poobal, S. (2015, February). Analysis of statistical texture features for automatic lung cancer detection in PET/CT images. In *2015 International Conference on Robotics, Automation, Control and Embedded Systems (RACE)*, 1-5. IEEE. Google Scholar↗

[24] Ronneberger, O., Fischer, P., & Brox, T. (2015, October). U-net: Convolutional networks for biomedical image segmentation. In *International Conference on Medical image computing and computer-assisted intervention*, 234-241. Springer, Cham. Google Scholar↗

[25] Sanz, H., Valim, C., Vegas, E., Oller, J. M., & Reverter, F. (2018). SVM-RFE: selection and visualization of the most relevant features through non-linear kernels. *BMC bioinformatics*, *19*(1), 1-18. Google Scholar↗

[26] Tekade, R., & Rajeswari, K. (2018, August). Lung cancer detection and classification using deep learning. In *2018 Fourth International Conference on Computing Communication Control and Automation (ICCUBEA)*, 1-5. IEEE. Google Scholar↗

[27] Tian, P., He, B., Mu, W., Liu, K., Liu, L., Zeng, H., ...& Li, W. (2021). Assessing PD-L1 expression in non-small cell lung cancer and predicting responses to immune checkpoint inhibitors using deep learning on computed tomography images. *Theranostics*, *11*(5), 2087-2098. Google Scholar↗

[28] Valente, I. R. S., Cortez, P. C., Neto, E. C., Soares, J. M., de Albuquerque, V. H. C., & Tavares, J. M. R. (2016). Automatic 3D pulmonary nodule detection in CT images: a survey. *Computer methods and programs in biomedicine*, *124*(1), 91-107. Google Scholar↗

[29] Vapnick, V. N. (1998). *Statistical learning theory*, Wiley, New York. *1*(1), 1-401. Google Scholar↗

[30] Zhang, F., Song, Y., Cai, W., Lee, M. Z., Zhou, Y., Huang, H., & Feng, D. D. (2013). Lung nodule classification with multilevel patch-based context analysis. *IEEE Transactions on Biomedical Engineering*, *61*(4), 1155-1166. Google Scholar↗

[31] Zhang, Q., Zhou, J., & Zhang, B. (2020, May). A noninvasive method to detect diabetes mellitus and lung cancer using the stacked sparse autoencoder. In *ICASSP 2020-2020 IEEE International Conference on Acoustics, Speech and Signal Processing (ICASSP)*, 1409-1413. IEEE. Google Scholar↗

[32] Verschakelen, J. A., Bogaert, J., & De Wever, W. (2002). Computed tomography in staging for lung cancer. *European Respiratory Journal*, *19*(35 suppl), 40S-48s. Google Scholar↗

****